Electronic Supporting Information

Synergism of molybdenum nitride and palladium for high-efficient formic acid electrooxidation

Haijing Yan, Yanqing Jiao, Aiping Wu, Chungui Tian,* Lei Wang, Xiaomeng Zhang and Honggang Fu*

Key Laboratory of Functional Inorganic Material Chemistry, Ministry of Education of the People's Republic of China, Heilongjiang University, Harbin 150080 (China)

The content of ESI

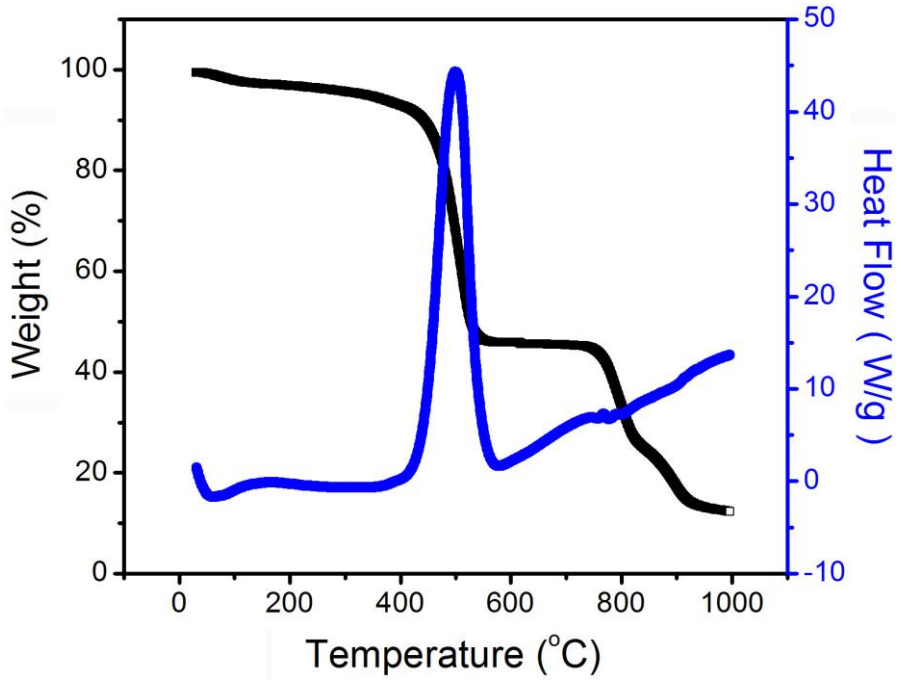

Figure S1. TG-DSC curve of Mo_2N/rGO under air atmosphere.

TG analysis was performed with a heating rate of 10 $^oC\ min^{-1}$ under air atmosphere. There is an obvious loss at the temperature of 450 ^oC, which may be ascribed to the decomposition of rGO support. In the process of calcination, the Mo_2N can be converted into the MoO_3 in company with the formation of carbon oxide (CO and CO_2) gases by the reaction of carbon in rGO with the air. The carbon oxide gases are released and the MoO_3 solid was left in the system. The amount of MoO_3 is about 48.1 wt.% as determined by TG analysis. The content of Mo_2N is about 35 wt.% calculated as below equation:

$$\mathbf{Mo_2N\ \% = MoO_3\ \% \times 204/144 \times 2}$$

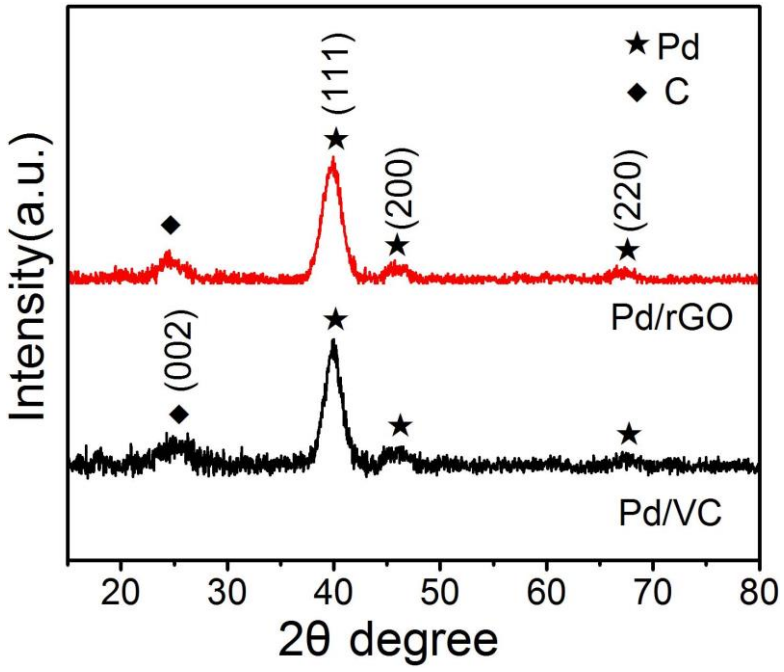

Figure S2. XRD patterns of Pd/rGO and Pd/VC.

Figure S2 shows the XRD patterns of Pd/rGO and Pd/VC. The peak at 26.5º is index to the (002) facet of graphite carbon. Three additional peaks at 40.2˚, 46.7˚ and 68.2˚ are correspond to (111), (200) and (220) facets of Pd (fcc), respectively. It is noted that a weak intensity of Pd phase was observed in Pd-Mo_2N/rGO (Figure 2a) relative to that in Pd/rGO and Pd/VC, indicating the possibly smaller sized Pd nanoparticles in the ternary hybrid.

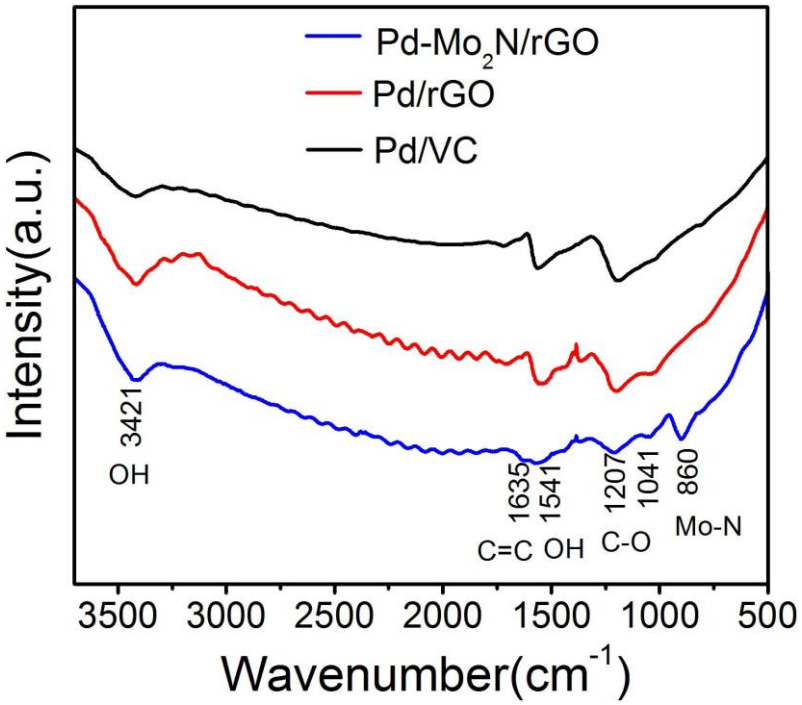

Figure S3. IR spectra of Pd/VC, Pd/rGO and Pd-Mo_2N/rGO.

In the spectra, the peaks at 3421 and 1541 cm^{-1} are assigned to the stretch vibration and bending vibration of water, respectively. The peaks at 1635 and 1207 cm^{-1} are index to the stretch vibration of C=C and C-O bonds in the carbon supports. The peak at 860 cm^{-1} is assigned to the stretch vibration of the Mo composites. In comparison with the results in Figure S3, the difference in the IR spectra of Pd-Mo_2N/rGO with Pd/rGO and Pd/VC is the existence of the Mo-N bond. The result further proves the successful preparation of the ternary Pd-Mo_2N/rGO composite.

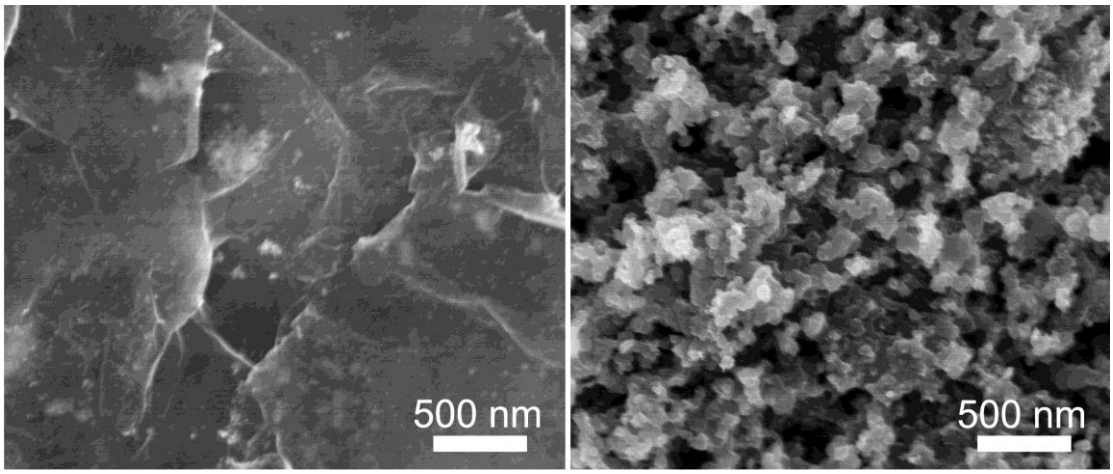

Figure S4. SEM images of (a) Pd/rGO and (b) Pd/VC.

In can be seen, the Pd NPs in the Pd/rGO and Pd/VC are large size with aggregation and worse uniformity than those in the Pd-Mo_2N/rGO. This result indicate the Mo_2N has an important role on the preventing the migration and aggregation of the Pd NPs on the rGO.

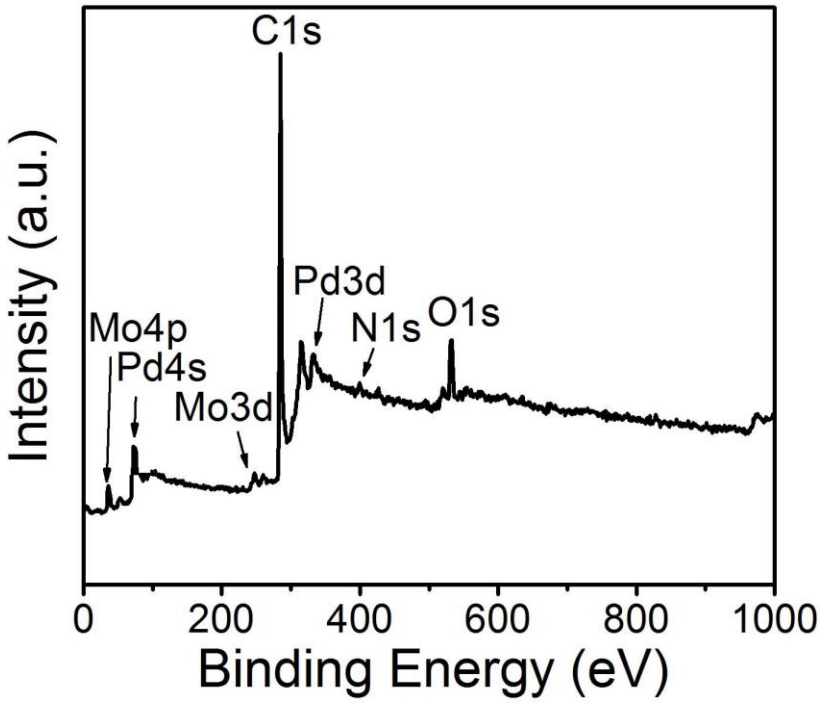

Figure S5. XPS survey spectrum of Pd-Mo_2N/rGO. The result reveals that the Pd-Mo_2N/rGO is mainly consisted of C, N, O, Mo and Pd elements.

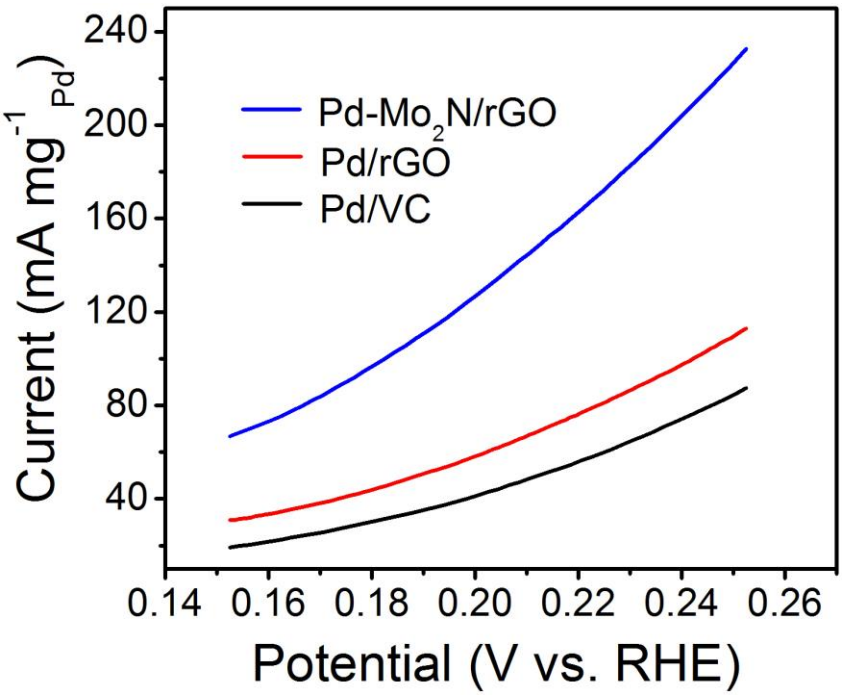

Figure S6. Formic acid electro-oxidation curves for catalysts at lower potential range.

The oxidation currents at the low potential (0.153 and 0.253 V) were given to evaluate the activity of the catalysts. The oxidation currents at 0.153 and 0.253 V for Pd-Mo_2N/rGO catalyst are 66.8 and 232.6 mA mg^{-1}_{Pd}, which are higher than those for Pd/rGO (30.6 and 112.9 mA mg^{-1}_{Pd}) and Pd/C (19.3 and 87.6 mA mg^{-1}_{Pd}) catalysts. The higher oxidation current at the low potential shows that Pd-Mo_2N/rGO catalyst has higher electrocatalytic performance compared to Pd/rGO and Pd/VC catalysts.

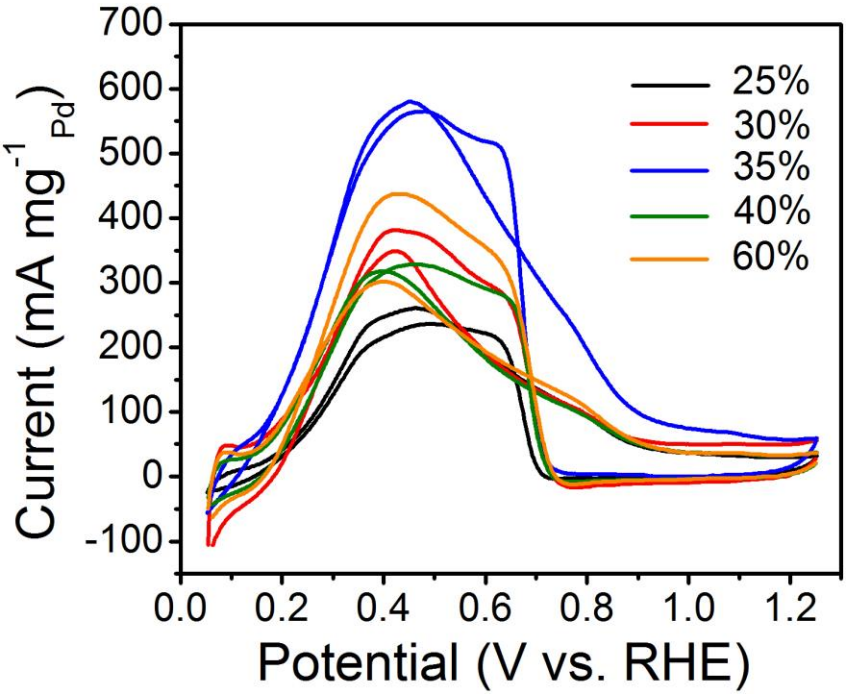

Figure S7. Formic acid electro-oxidation curves for the Pd-Mo_2N/rGO catalysts with the varying contents of Mo_2N recorded in aqueous 0.5 M H_2SO_4 + 0.5 M HCOOH solution with a scan rate of 50 mV s^{-1}.

To further investigate the possibility of the enhancement effect of Mo_2N on the intrinsic electrocatalytic activity, the relationship of Mo_2N content and electroactivity was performed. As shown in Figure S7, the Pd-Mo_2N/rGO with different contents (25%, 30%, 35% 40% and 60%) of Mo_2N on rGO are synthesized to investigate the effects of Mo_2N content toward to electrocatalytic activity of FAOR. With the dose of Mo_2N increasing, the electrocatalytic activity of Pd-Mo_2N/rGO presents a "volcano shape". The Pd-Mo_2N/rGO catalyst with 35 wt% of Mo_2N on rGO exhibits an especially high current density of 532.7 mA mg^{-1}_{Pd}. Both Mo_2N content too low and too high are unfavorable for catalytic performance to play, which may be due to that when Mo_2N content too low, Mo_2N is not a good contact with the palladium to play the synergistic effect while when Mo_2N content too high, this inevitably brings Mo_2N aggregation. This result indicates that an appropriate loading amount of Mo_2N is important to produce Pd-Mo_2N/rGO with outstanding activity.

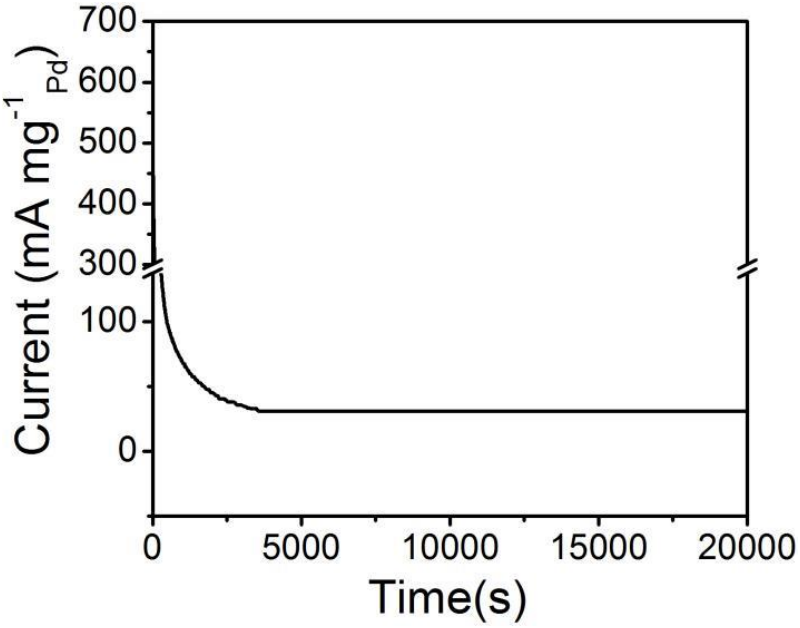

Figure S8. Chronoamperometric curve of Pd-Mo_2N/rGO catalyst after 20000 s.

The CA test at longer time (20000 s) was as shown in Figure S8. The current is about 31.7 mA mg^{-1}_{Pd} after test of 20000 s, and it is obvious that the current reaches a stable value after 3600 s. The result further demonstrates the good stability of Pd-Mo_2N/rGO catalyst.

Table S1. Performance comparison with recent reported Pd-based catalysts in the literature.

Catalysts	The activity ratio of the catalysts and Pd/carbon	Reference
Pd/N-C	1.96	1
Pd4Ir@G	2.02	2
Pd@Graphene	1.36	3
Pd-Fe_3O_4/C	2.82	4
PdCu	1.41	5
Pd/NS-G	1.48	6
Pd/WO_3/C-APTMS	1.42	7
Pd-Mo_2N/rGO	2.20	This work

[1] J. F. Chang, X. J. Sun , L. G. Feng, W. Xing, X. J. Qin, G. J. Shao, *J Power Sources*, 2013, **239,** 94-102.
[2] L. Y. Zhang, Z. Liu, *J Colloid Interf. Sci.*, 2017, **505,** 783-788.
[3] L. Y. Zhang, Z. L. Zhao, C. M. Li, *Nano Energy*, 2015, **11,** 71-77.
[4] P. C. Meléndez-González, J. C. Carrillo-Rodríguez, D. Morales-Acosta, S. Mukherjee, F. J. Rodríguez-Varela, *Int J Hydrogen Energy*, 2017, **42,** 30284-30290.
[5] D. Chen, P. C. Sun, H. Liu, J. Yang, *J. Mater. Chem. A*, 2017, **5,** 4421-4429.
[6] J. W. Chen, G.Wang, X. Q. Wang, C. P. Jiang, S. F. Zhu, R. L. Wang, *J Mater. Res.*, 2013, **28,**1553-1558.
[7] Y. Yang, Y, H. Li, Y. F. Zhao, P. W. Li, Q. X. Li, *J Nanopart. Res.*, 2018, **20,** 12.